JMEPEG (1993) 2:271-282

R-Adapted Arbitrary Lagrangian-Eulerian Finite-Element Method in Metal-Forming Simulation

S. Ghosh and S.K. Manna

In this article, mesh adaptation techniques have been used with the arbitrary Lagrangian-Eulerian finite-element method for analysis of metal-forming problems. The *r*-method of node relocation has been found suitable for this purpose and is driven by errors based on effective plastic strain. Two forming simulations for elastic-viscoplastic materials have been executed under plane-strain conditions, and the effect of mesh adaptation has been studied.

Keywords
finite element, Lagrangian-Eulerian method, plasticity, stress, strain

1. Introduction

DURING the last decade, the arbitrary Lagrangian-Eulerian (ALE) kinematic description has been used successfully to analyze large deformation of solids by the finite-element method. This description has been successful in circumventing some of the major obstacles encountered in the pure Lagrangian or Eulerian descriptions, such as severe localized mesh distortion, inadequate contact boundary representation, inaccuracy in the depiction of substantially moving complex boundaries, etc. The ALE description introduces a reference frame, which may be in any arbitrary spatial motion, to impart the flexibility required by the finite-element mesh for large deformation analysis, especially in metal-forming simulation. It is capable of representing pure Lagrangian or Eulerian descriptions in the limit, wherever required. This powerful description has been used to execute large deformation analysis of elastic-plastic solids in an explicit setting by Haber;[1] Liu, Belytschko, and Chang;[2] Huetink, Lugt, and Vreede;[3] and Ponthot;[4] and by Ghosh and Kikuchi[5] for elastic-viscoplastic solids using implicit time integration. Among the direct applications of this method to metal-forming problems are the work of Ghosh,[6] who has exhibited its potential in extrusion problems and that of Hu and Liu,[7] who have performed ring rolling simulation.

Despite the flexibility of the finite-element mesh in the ALE description, the additional degrees of freedom introduced can pose difficulties while simulating complex problems. When the motion of the mesh is prescribed by the user of a complicated process simulation, the ALE model can be adversely affected from considerations of accuracy. Lack of knowledge about the sensitivity of solutions to the grid configuration can deteriorate the quality of the finite-element solutions. Grid adaptation procedures involve optimal design of the mesh, based on minimizing finite-element approximation error due to discretization. The obstacles in the ALE method can therefore be surpassed by using the freedom of the grid motion as a tool for reducing the errors incurred through improper positioning or distortion of the mesh. In this article, an amalgamation of grid adaptation methods with the ALE description has therefore been attempted to simulate metal-forming problems.

Extensive research has been done on finite-element mesh adaptation of linear systems since the late 1970s. They involved methods like *r*-adaptation, *h*-adaptation, and the *p*-adaptation. The extension to nonlinear solid mechanics is, however, much less developed. This may be attributed to the difficulty in establishing methods of error analysis for nonlinear problems. Kikuchi and Cheng[8] have introduced adaptive methods in elastic-plastic metal-forming problems by applying *r*- and *h*-methods. Zienkiewicz, Liu, and Huang[9] have applied adaptive methods to the simulation of metal-forming problems using a flow formulation. Their adaptive schemes subdivide elements locally or regenerate the total mesh on the basis of an error estimator expressed as the ratio between error in the energy norm and the energy norm.

In another article, Huang, Liu, and Zienkiewicz[10] introduced the concept of an analytical mesh for finite-element analysis and a material grid for output display. After refinement by *h*-adaptive methods, the analytical mesh is updated according to the prescribed mesh velocities, which are different from the material velocities. Kikuchi and Torigaki[11] applied adaptive methods to large deformation plasticity/viscoplasticity for impact and contact problems with the Lagrangian description. Bass and Oden[12] have developed several error indicators based on interpolation theory or more physical entities for a broad class of small deformation problems in viscoplasticity.

In the present study, the implicit ALE finite model of Ghosh and Kikuchi[5] has been enhanced with adaptive mesh movement capability. A two-dimensional plane-strain model has been considered for this purpose. Incremental and accumulated forms of interpolation error in the effective viscoplastic strain and domain boundary error due to stretching have been instrumental in monitoring the mesh movement by the *r*-method of node relocation.

2. Review of the ALE Model

The arbitrary Lagrangian-Eulerian description introduces a reference configuration, consisting of a set of unconstrained

S. Ghosh, Department of Engineering Mechanics, The Ohio State University, Columbus, Ohio; and **S.K. Manna**, Department of Engineering Mechanics, The University of Alabama, Tuscaloosa, Alabama.

grid points that undergo arbitrary spatial motion. Each point in this reference configuration is unambiguously represented by an invariant set of three independent coordinates χ_i. The motion of points in the reference frame is denoted by the set of spatial coordinates, x_i, and is expressed as arbitrary continuous functions of χ_i and time, t. The conservation laws of mechanics may then be written as:

Continuity:

$$\frac{\partial(\rho J)}{\partial t}\Big|_{\chi} + J\frac{\partial}{\partial x_i}[\rho(V_i - W_i)] = 0 \qquad [1]$$

Momentum:

$$\rho G_i + \frac{\partial \sigma_{ji}}{\partial x_j} = \rho \frac{\partial V_i}{\partial t}\Big|_{\chi} + \rho(V_j - W_j)\frac{\partial V_i}{\partial x_j} \qquad [2]$$

Energy:

$$\rho\frac{\partial \hat{u}}{\partial t}\Big|_{\chi} + \rho(V_j - W_j)\frac{\partial \hat{u}}{\partial x_j} = \sigma_{ji}D_{ji} - \frac{\partial q_i}{\partial x_i} + f \qquad [3]$$

where $\boldsymbol{W}$ refers to the velocity of a representative grid point; $\boldsymbol{V}$ refers to the velocity of the material point coinciding with the grid at time, t; $\hat{u}$, is the specific internal energy; $\boldsymbol{D}$ is the rate of deformation; σ_{ij} is the Cauchy stress tensor; ρ is the density; $\boldsymbol{G}$ is the body force per unit mass; f is the internal heat source; $\boldsymbol{q}$ is the heat flux; and J is the Jacobian.

The material characteristics for the deforming bodies are described using a rate-dependent elastic-viscoplastic model for finite deformation in a rotated Lagrangian system. In this system, the constitutive relation is expressed as:

$$\dot{\boldsymbol{t}} = \boldsymbol{E}:(\boldsymbol{d} - \boldsymbol{d}^{vp}) \qquad [4]$$

In Eq 4, $\dot{\boldsymbol{t}}$ is the material time derivative of a rotated stress tensor, $\boldsymbol{t}$, that is obtained by rotation of the Cauchy stress tensor σ by the rotation tensor, $\boldsymbol{R}$, which is derived from the polar decomposition of the deformation gradient tensor. $\boldsymbol{d}$ is the corresponding rotated rate of deformation tensor, and $\boldsymbol{E}$ is a fourth-order elasticity tensor. The viscoplastic deformation rate, d^{vp}, is characterized by a unified overstress model as:

$$d_{ij}^{vp} = \gamma\langle\Phi[\bar{t} - \kappa(W_p)]\rangle\frac{\partial \bar{t}}{\partial t_{ij}} \qquad [5]$$

in which γ is the viscosity coefficient; $\langle\rangle$ is the MacCaulay operator; κ is the internal state variable, which is a function of the inelastic work, W_p; and $\bar{t}$ is an effective stress measure. The function Φ may be chosen to fit characteristics of the material being modeled. The relation between the work-hardening parameter κ and the effective viscoplastic strain rate $\bar{d}^{vp}$ is expressed as:

$$\frac{\partial \kappa}{\partial t} = E_p\bar{d}^{vp} \qquad [6]$$

where E_p is an equivalent viscoplastic modulus.

Evaluation of process variables at nodal points in an ALE description requires an additional relation for updating values from material points to grid points. Such an equation correlates time derivatives of a material variable in fixed material coordinates to that in fixed referential coordinates. Thus, if β is a time-dependent material variable, the rates in the two coordinate systems are related as:

$$\frac{\partial \beta}{\partial t}\Big|_{\chi} = \frac{\partial \beta}{\partial t}\Big|_{X} + (W_k - V_k)\frac{\partial \beta}{\partial x_k} \qquad [7]$$

where $\left(\frac{\partial}{\partial t}\right)\Big|_X$ and $\left(\frac{\partial}{\partial t}\right)\Big|_{\chi}$ refer to material and referential time derivatives, respectively.

The boundaries of the deforming bodies are assumed to be entirely constituted of displacement, traction, and contact parts, that is, $\Gamma(t)$ is $\Gamma_{iu}(t) \cup \Gamma_{iT}(t) \cup \Gamma_{ic}(t)$ for $1 \le i \le 3$. In this analysis, all contact surfaces are assumed to be frictionless. The developments in normal contact algorithms are based on an exterior penalty function. The normal contact stress $T_n(= \sigma_{ij}n_in_j)$ can then be evaluated through a penalization of the impenetrability constraint condition as:

$$-T_n = \frac{1}{\varepsilon_n}\langle p\rangle \qquad [8]$$

where the penalty parameter ε_n is a sufficiently small number, and p is the gap function.

3. Error Estimation and Adaptive Strategy

Error measure of any suitably chosen function in an element Ω_e may be defined as:

$$E_e = ||f(\boldsymbol{u} - \boldsymbol{u}^h)|| \qquad [9]$$

where u is the true solution; u^h is its finite-element approximation; and f is any appropriate function of displacement such as energy, stress, or strain, and $||\cdot||$ denotes a norm of the function. In general, for large deformation problems, two types of errors arising from spatial discretization have been used. They are:

- Error due to finite-element approximation of the solution, i.e., displacement
- Error due to finite-element approximation of the domain

In an incremental analysis, the first type of error within each increment is similar to that in small deformation problems because of linearization. The second type of error is only significant for large deformation problems due to substantial stretching of elements. These stretched elements may not closely reflect the shape of the true undeformed domain and may cause significant domain integration error due to the difference between the discretized and actual domains.

Large deformation problems generally are characterized by large plastic flow and hence the plastic strain, because a large amount of energy is dissipated through plastic work. The first type of error measure can therefore be formulated using effective viscoplastic strain for the error function f as:

$$E_e = \left\{\int_{\Omega_e}\left[\bar{\varepsilon}^{vp}(\boldsymbol{u} - \boldsymbol{w}^h)\right]^2 d\Omega\right\}^{1/2} \qquad [10]$$

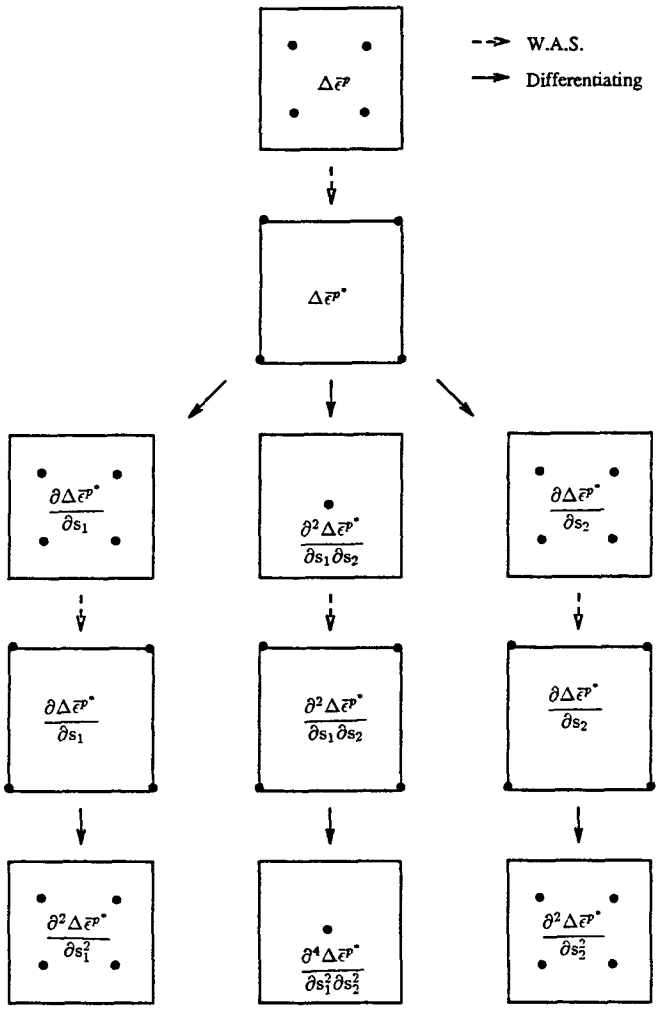

Fig. 1 Evaluation of terms in the interpolation error.

where $\bar{\varepsilon}^{vp}$ denotes total effective viscoplastic strain; $\boldsymbol{u}$ is the actual displacement field, and $\boldsymbol{w}^h$ is its interpolation. This interpolation error represents the effective viscoplastic strain due to the difference between the true displacement and its interpolated value. The corresponding incremental error within a time interval is:

$$\Delta E_e = \left\{ \int_{\Omega_e} [\Delta\bar{\varepsilon}^{vp}(u - w^h)]^2 d\Omega \right\}^{1/2} \quad [11]$$

where $\Delta\bar{\varepsilon}^{vp}$ denotes an increment of effective viscoplastic strain.

The domain error is due to considerable stretching of elements, especially near the boundary. Because the norm of effective viscoplastic strain is a good indicator of elements stretching, the second type of error indicator corresponding to accumulated strain can be defined as:

$$E_e = \left\{ \int_{\Omega_e} \left[\bar{\varepsilon}^{vp}(u)\right]^2 d\Omega \right\}^{1/2} \quad [12]$$

and its incremental form in a time increment is given by:

$$\Delta E_e = \left\{ \int_{\Omega_e} [\Delta\bar{\varepsilon}^{vp}(u)]^2 d\Omega \right\}^{1/2} \quad [13]$$

To obtain a generalized error indicator, both the sources of error can be combined into a single expression to yield an effective accumulated error:

$$E_e = \left\{ \left[\int_{\Omega_e} \left[\bar{\varepsilon}^{vp}(u - w^h)\right]^2 d\Omega \right]^{m/2} \left[\int_{\Omega_e} \left[\bar{\varepsilon}^{vp}(u)\right]^2 d\Omega \right]^{n/2} \right\}^{1/m+n} \quad [14]$$

where the exponents m and n denote weights for the two error sources. The corresponding combined incremental error then takes the form:

$$\Delta E_e = \left\{ \left[\int_{\Omega_e} \left[\Delta\bar{\varepsilon}^{vp}(u - w^h)\right]^2 d\Omega \right]^{m/2} \left[\int_{\Omega_e} \left[\Delta\bar{\varepsilon}^{vp}(u)\right]^2 d\Omega \right]^{n/2} \right\}^{1/m+n} \quad [15]$$

In this study, various combinations of m and n have been experimented with to investigate their effect on mesh adaptation. Details of the above error estimates may be found in Torigaki.[13]

3.1 *Simplified Form of Error Estimators*

It has been shown by Torigaki[13] that $\boldsymbol{u} - \boldsymbol{w}^h$ can be approximated by $\boldsymbol{u}^* - \boldsymbol{u}^h$ where $\boldsymbol{u}^*$ is a smoother function obtained from $\boldsymbol{u}^h$. Therefore, $\Delta\bar{\varepsilon}^{vp}(\boldsymbol{u} - \boldsymbol{w}^h)$ in Eq 15 can be replaced by $\Delta\bar{\varepsilon}^{vp}(\boldsymbol{u}^* - \boldsymbol{u}^h)$, which can be approximated by derivatives of $\boldsymbol{u}^*$. Using a Taylor series expansion, $\boldsymbol{u}^*$ can be approximated at a point s^0 in the local coordinate system (s_1, s_2) of a QUAD4 element as:

$$\begin{aligned} \boldsymbol{u}^*(s)\big|_{s^0} &= u^*(s) + (s_1^0 - s_1)\frac{\partial u^*(s)}{\partial s_1} + (s_2^0 - s_2)\frac{\partial u^*(s)}{\partial s_2} \\ &+ \frac{1}{2}(s_1^0 - s_1)^2 \frac{\partial^2 u^*(s)}{\partial s_1^2} + \frac{1}{2}(s_2^0 - s_2)^2 \frac{\partial^2 u^*(s)}{\partial s_2^2} \\ &+ (s_1^0 - s_1)(s_2^0 - s_2)\frac{\partial^2 \boldsymbol{u}^*(s)}{\partial s_1 \partial s_2} + \frac{1}{2}(s_1^0 - s_1)^2(s_2^0 - s_2)\frac{\partial^3 \boldsymbol{u}^*(s)}{\partial s_1^2 \partial s_2} \\ &+ \frac{1}{2}(s_1^0 - s_1)(s_2^0 - s_2)^2 \frac{\partial^3 \boldsymbol{u}^*(s)}{\partial s_1 \partial s_2^2} + \frac{1}{4}(s_1^0 - s_1)^2(s_2^0 - s_2)^2 \frac{\partial^4 \boldsymbol{u}^*(s)}{\partial s_1^2 \partial s_2^2} \\ &+ \text{Higher order terms.} \quad -\boldsymbol{u}^*(s) \text{ in } \Omega_e \end{aligned} \quad [16]$$

Using an isoparametric interpolation for the QUAD4 element, u^h is written as:

$$u^h(s) = u^*(s)|_{-1,-1}\frac{1}{4}(1-s_1)(1-s_2) + u^*(s)|_{1,-1}\frac{1}{4}(1+s_1)(1-s_2) + u^*(s)|_{1,1}\frac{1}{4}(1+s_1)(1+s_2) + u^*(s)|_{-1,1}\frac{1}{4}(1-s_1)(1+s_2) \quad [17]$$

Substituting Eq 17 into 16 yields:

$$u^* - u^h = \frac{1}{2}\frac{\partial^2 u^*(s)}{\partial s_1^2}(s_1^2-1) + \frac{1}{2}\frac{\partial^2 u^*(s)}{\partial s_2^2}(s_2^2-1) - \frac{1}{4}\frac{\partial^4 u^*(s)}{\partial s_1^2 \partial s_2^2}(s_1^2-1)(s_2^2-1) \quad [18]$$

In expression 18, u^* has the same properties as a biquadratic polynomial in a QUAD9 element. For sufficiently small increments, the assumption of linearity of $\Delta\bar{\varepsilon}^{vp}$ with respect to $(u^* - u^h)$ leads to the following approximation:

$$\Delta\bar{\varepsilon}^{vp}(u^* - u^h) \approx \Delta\bar{\varepsilon}^{vp}(u^*) - \Delta\bar{\varepsilon}^{vp}(u^h) \approx \frac{1}{2}\frac{\partial^2 \Delta\bar{\varepsilon}^{vp*}}{\partial s_1^2}(s_1^2-1) + \frac{1}{2}\frac{\partial^2 \Delta\bar{\varepsilon}^{vp*}}{\partial s_2^2}(s_2^2-1) - \frac{1}{4}\frac{\partial^4 \Delta\bar{\varepsilon}^{vp*}}{\partial s_1^2 \partial s_2^2}(s_1^2-1)(s_2^2-1) \quad [19]$$

where $\Delta\bar{\varepsilon}^{vp*}$ denotes $\Delta\bar{\varepsilon}^{vp}(u^*)$. Equation 19 can be evaluated at element integration points by using the least-squares method or weighted averaging schemes. The method of calculating the derivatives are shown in Fig. 1.

Because the effective viscoplastic strains and their interpolation errors in the equation for the accumulated error equation (Eq 14) are material variables, they should be updated to the grid integration points of the subsequent configurations in each time step in the ALE finite-element model. This has been achieved by integrating Eq 7 with β substituted by the appropriate material variable.

$$\bar{\varepsilon}^{vp^{n+1}}(u^h) = \bar{\varepsilon}^{vp^n}(u^h) + \Delta^m\bar{\varepsilon}^{vp}(u^h) + \Delta t(W_k^{n+\alpha} - V_k^{n+\alpha})\left(\frac{\partial\bar{\varepsilon}^{vp}(u^h)}{\partial x_k}\right)^{n+\alpha}$$

$$\bar{\varepsilon}^{vp^{n+1}}(u^* - u^h) = \bar{\varepsilon}^{vp^n}(u^* - u^h) + \Delta^m\bar{\varepsilon}^{vp}(u^* - u^h) + \Delta t(W_k^{n+\alpha} - V_k^{n+\alpha})\left(\frac{\partial\bar{\varepsilon}^{vp}(u^* - w^h)}{\partial x_k}\right)^{n+\alpha} \quad [20]$$

where $\Delta^m\bar{\varepsilon}^{vp}(u^h)$ and $\Delta^m\bar{\varepsilon}^{vp}(u^* - u^h)$ correspond to respective increments at a fixed material point; Δt is the time increment; W is the grid velocity; and V is the material velocity. $\bar{\varepsilon}^{vp^{n+1}}(u^h)$ and $\bar{\varepsilon}^{vp^{n+1}}(u^* - u^h)$ are, respectively, the updated effective viscoplastic strain and its interpolation error at element integration points in the $(n+1)$-th configuration. The accumulated error (Eq 14) can then be evaluated using the Gaussian quadrature integration.

3.2 *Mesh Adaptation Scheme*

Following the evaluation of an error indicator, an adaptation technique is applied for improving the accuracy of the results. The *r*-method of node relocation is a natural choice with the ALE description, because it can use the flexibility of the grid motion. In this method, the finite-element mesh is modified by the relocation of its nodal coordinates according to the solution of an optimal grid design problem stated as:

$$\text{Minimize}\left[\begin{matrix}\text{Max} & \{E_e\} \\ e = 1, \ldots N_E\end{matrix}\right] \quad \text{by } \textit{adaptive method} \quad [21]$$

where E_e is the error indicator in element Ω_e, and N_E is the total number of elements. Kikuchi,[14] Diaz, Kikuchi, and Taylor;[15] and Demkowicz and Oden[16] have proven that the necessary condition for the above min-max problem is:

$$E_e = \text{Constant} \qquad \text{for } e = 1, \ldots N_E \quad [22]$$

i.e., the optimal mesh for a fixed number of elements is obtained by equidistribution error indicators among all elements in the domain.

Following the work of Torigaki,[13] an iterative scheme is implemented for determining the new nodal coordinates based on the *r*-method. This is because a given error measure depends on the shape and size of the elements and the finite-element solution u^h, all of which are likely to change as a result of node relocation. Assuming that the node relocation affects only the characteristic size of an element and not the overall element location, an iteration invariant, D_e, may be defined as:

$$D_e = \left(\frac{E_e}{h^{k+r}}\right)_{\text{before}} \approx \left(\frac{E_e}{h^{k+r}}\right)_{\text{after}} \quad [23]$$

where h is the characteristic size of an element Ω_e; $k \geq 1$ is the degree of finite-element interpolation function; and r is the power due to integration over an element Ω_e. For the two-dimensional case, r assumes of value of 1. If the design variable L_e is the area of an element Ω_e, then D_e may be redefined as:

$$D_e = \frac{E_e}{L_{o_e}^{\alpha}}$$

where L_{o_e} is the area before the node relocation, and the parameter $\alpha = \frac{1}{2}(k+1) = 1$ for the two dimensional case. Consequently, the error measure after relocation becomes:

$$\hat{E}_e = D_e L_e^{\alpha}$$

With this assumption, the necessary condition (Eq 22) can be redefined as:

$$\hat{E}_e = \text{Constant} \qquad \text{for } e = 1, \ldots N_E \quad [24]$$

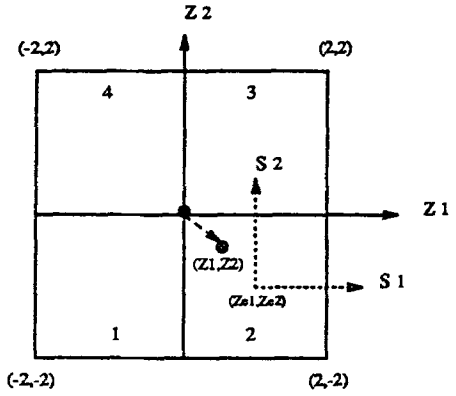

Fig. 2 Node relocation in special domain.

A node relocation procedure, suggested by Diaz et al.,[15] has been effective in approximately satisfying the optimality condition and hence is adopted in this work. According to this scheme, the new coordinates x of the relocated node are derived according to a weighted averaging scheme as:

$$x = \frac{\sum_{e=1}^{NRE} x_e D_e L_e^{\alpha-1}}{\sum_{e=1}^{NRE} D_e L_e^{\alpha-1}} \qquad [25]$$

where x_e is the coordinates of the center of elements that share the node, and *NRE* denotes the total number of such elements. This scheme, however, may not lead to the optimality condition if the surrounding elements are not regular. In such cases, Eq 25 will relocate nodes even if $D_e L_e^{\alpha}$ in the surrounding elements are the same. In large deformation problems, irregular elements occur frequently, and hence, a modified form of Eq 25 has been considered for node relocation. In this approach, nodes are relocated in a special domain and then transformed to the physical domain, as suggested by Torigaki.[13] The domain consists of identical elements surrounding the node to be relocated, as shown in Fig. 2. In the present study, only four surrounding elements have been considered for each internal node, and hence, these elements have been assumed to be unit squares. In the event that different numbers of elements surround each node, the shape of these elements will be different. A local coordinate system z is introduced with its origin at the node to be relocated such that the coordinates of centroids of the surrounding elements are fixed in this system (z_1,z_2). Then, the new relocation procedure is written as:

$$z = \frac{\sum_{e=1}^{NRE} z_e D_e L_e^{\alpha}}{\sum_{e=1}^{NRE} D_e L_e^{\alpha}} \qquad [26]$$

where z is the coordinate of the relocated node in the special domain. It is important to note that it is vital to retain the order of connectivity of surrounding elements in the special domain corresponding to that in physical domain. The element that contains the new nodal coordinate z is then identified. A second coordinate system (s_1,s_2), with its origin at the centroid of the element in the special domain, is now introduced. If (z_{e_1}, z_{e_2}) are the centroidal coordinates of the element, then corresponding new coordinates can be obtained by:

$$s_1 = z_1 - z_{e_1}$$
$$s_2 = z_2 - z_{e_2} \qquad [27]$$

The physical coordinates x of the relocated node are then obtained from s by usual isoparametric transformation for QUAD4 elements.

If the values of error measure in the surrounding elements vary considerably, the node relocation process can become oscillatory. The error measures are therefore scaled to stabilize this effect. Another aspect that requires special attention in the mesh adaptation procedure for the elastic-viscoplastic case is when adjacent elements have not all yielded. Because effective viscoplastic strain determines the error in an element, the error indicators are zero in an elastic element. Application of Eq 26 in this case will result in an excessive node relocation toward the plastic element because of the jump in error indicator. In such cases, nodes have been relocated only along the elastic-plastic interface based on errors in plastic elements. A similar technique also can be applied for relocating boundary nodes. Nodes that are relocated by the adaptive scheme in an intermediate configuration are then accommodated in ALE formulation through Eq 1, 2, and 7, as detailed in Ref 5 and 17.

4. Numerical Examples

Plane-strain analysis has been carried out for two examples of metal-forming problems discussed with different values assigned to m and n in Eq 14 and 15, as outlined in Fig. 3.

In metal-forming problems that involve sharp changes in the directions of material flow, mesh adaptation schemes based on error analysis alone fail to alleviate the severe mesh distortion, particularly at zones of localized deformation. Various combinations of the r-method and different automatic mesh generation procedures consequently have been applied to overcome the distortions and to continue the simulations. In Fig. 3, MG denotes mesh generators. In particular, a local algebraic generator based on serendipity interpolation functions and a transfinite mapping method have proved to be effective in these cases. For simulations with transfinite mapping mesh movement, a convex combination of two effects governs the effective motion of nodes. Let Δx_{tran} and Δx_{adapt} be the calculated node displacements by pure transfinite mapping and pure r-adaptation, respectively. The resulting motion of a node is then taken to be:

$$\Delta x = w \cdot \Delta x_{adapt} + (1 - w) \cdot \Delta x_{tran}$$

where $w (0 \le w \le 1)$ is a weighting factor. The effect of each criterion can be controlled by assigning different values of w at various regions of the domain.

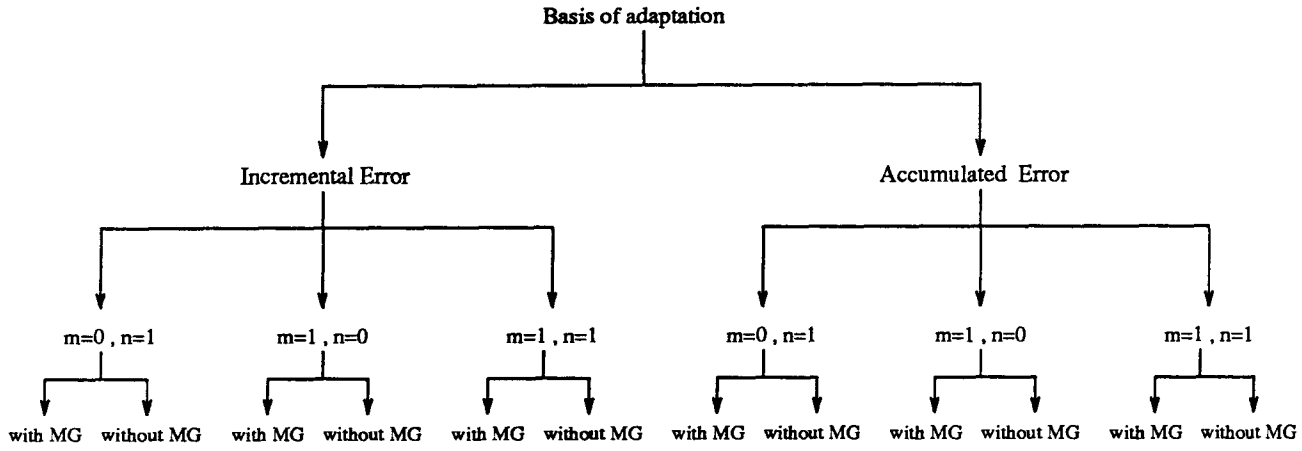

Fig. 3 Summary of different cases of adaptation.

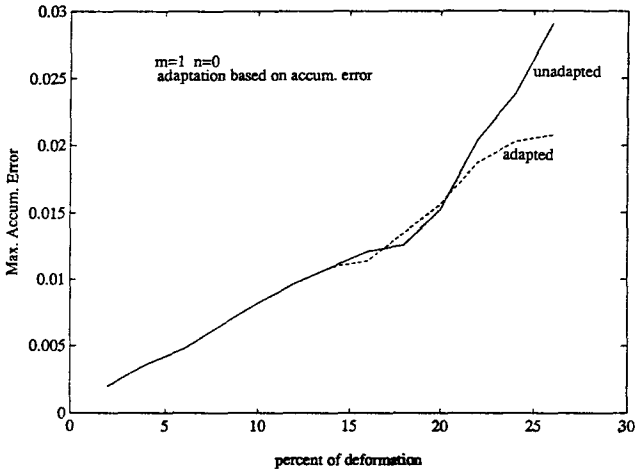

Fig. 4 Comparison of maximum accumulated error for adapted/unadapted backward extrusion ($m = 1, n = 0$).

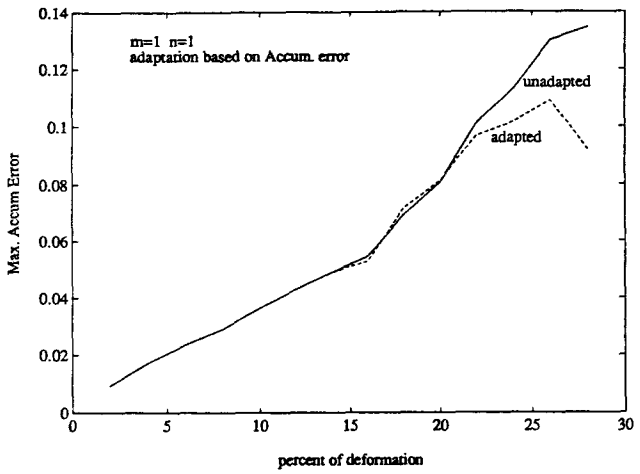

Fig. 5 Comparison of maximum accumulated error for adapted/unadapted backward extrusion ($m = 1, n = 1$).

4.1 *Backward Extrusion*

In this problem, a rigid prismatic punch is extruding a billet of rectangular cross section at a rate of 10 in./s for 0.25 s. During this time, the height of the billet under the punch is expected to reduce by 50% of its original value. The contact surfaces between the worktools (punch or die) and the workpiece (billet) are assumed to be frictionless. The material of the billet is elastic-viscoplastic with the following properties:

Young's modulus (E) = 10×10^7 psi
Poisson's ratio (ν) = 0.3
Yield stress (σ_Y) = 0.16×10^5 psi
Elastic-plastic tangent modulus (E_p) = 0.526315×10^6 psi
Viscosity coefficient (γ) = 0.001/s

Similar problems have been solved by Cheng and Kikuchi[18] using a mesh rezoning technique for elastic-plastic material and by Ghosh[6] and Ghosh and Kikuchi[5] by applying the ALE finite-element method. Analysis was carried out for all combinations of m and n (taking values 0 or 1) for both incremental and accumulated error criteria. Figures 4 and 5 show the variation of maximum accumulated error within the domain as a function of the deformation for simulations with and without r-adaptation for $m = 1$, $n = 0$ and $m = 1$, $n = 1$, respectively. Adaptation starts when the punch has moved down by 16% of the initial billet height and is executed every 2% displacement thereafter. As expected, the maximum error is considerably lower in the cases of adapted simulation. However, as mentioned earlier, severe distortion of elements near the edge of the punch leads to difficulties in continuation beyond 25% deformation.

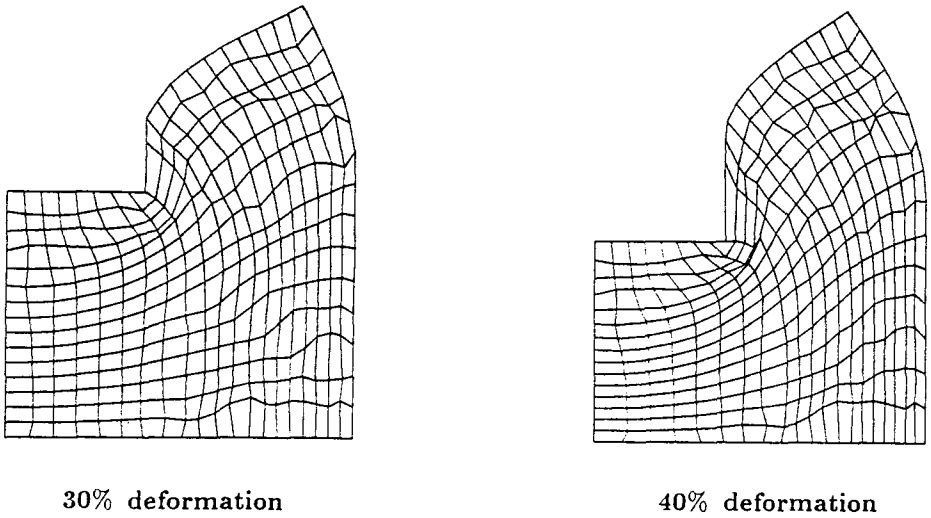

Fig. 6 Mesh movement in backward extrusion with *r*-adaptation and algebraic generator.

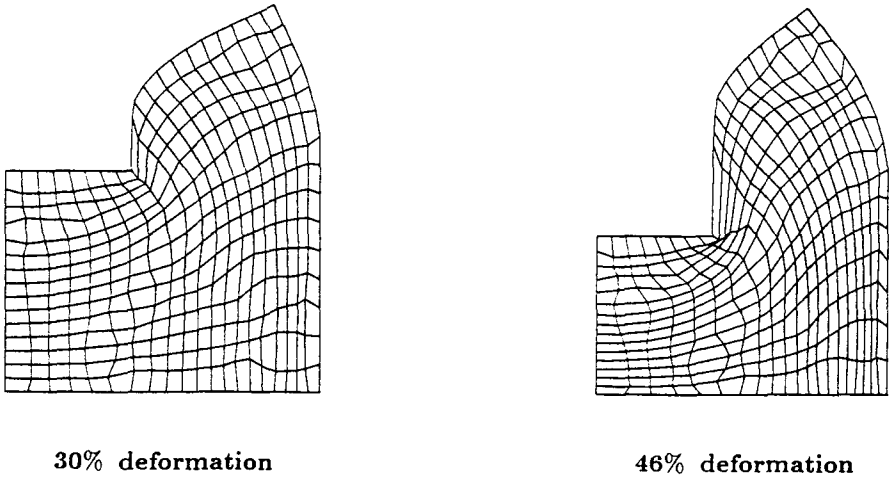

Fig. 7 Mesh movement in backward extrusion with *r*-adaptation and transfinite mapping.

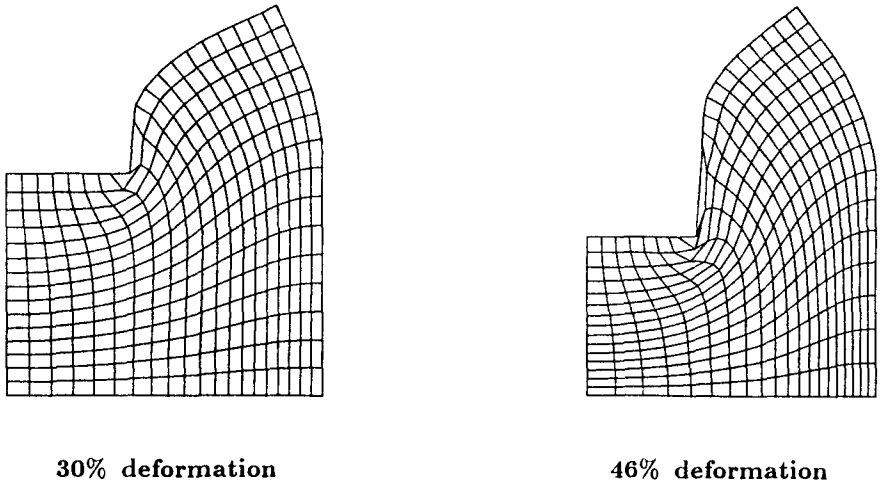

Fig. 8 Material motion in backward extrusion.

A local serendipity algebraic mesh generator consequently has been applied near the edge to surpass such distortion. The resulting mesh patterns for $m = 1$, $n = 1$ and adaptation based on incremental error are shown in Fig. 6. Satisfactory results, in terms of degree of deformation, were achieved in the simulation for $m = 1$, $n = 1$, with adaptation based on accumulated error coupled with transfinite mapping. The value of the weight factor w was varied from 0.25 near the punch to 0.6 away from it.

Figure 7 shows the adapted mesh patterns at 30 and 46% deformation, whereas Fig. 8 demonstrates the corresponding material configurations. Comparison of these figures shows the nonconvex material elements near the edge, whereas the finite-element grid maintains its convexity. Figure 9 shows the equivalent stress and effective viscoplastic strain distribution in the material at 46% deformation. Distribution of incremental and accumulated errors in the domain at 46% deformation is shown in Fig. 10. The variation in incremental and accumulated errors with deformation are depicted in Fig. 11. It can be inferred from Fig. 11 that adaptations based on either accumulated or incremental errors yield almost the same levels of total errors in the domain.

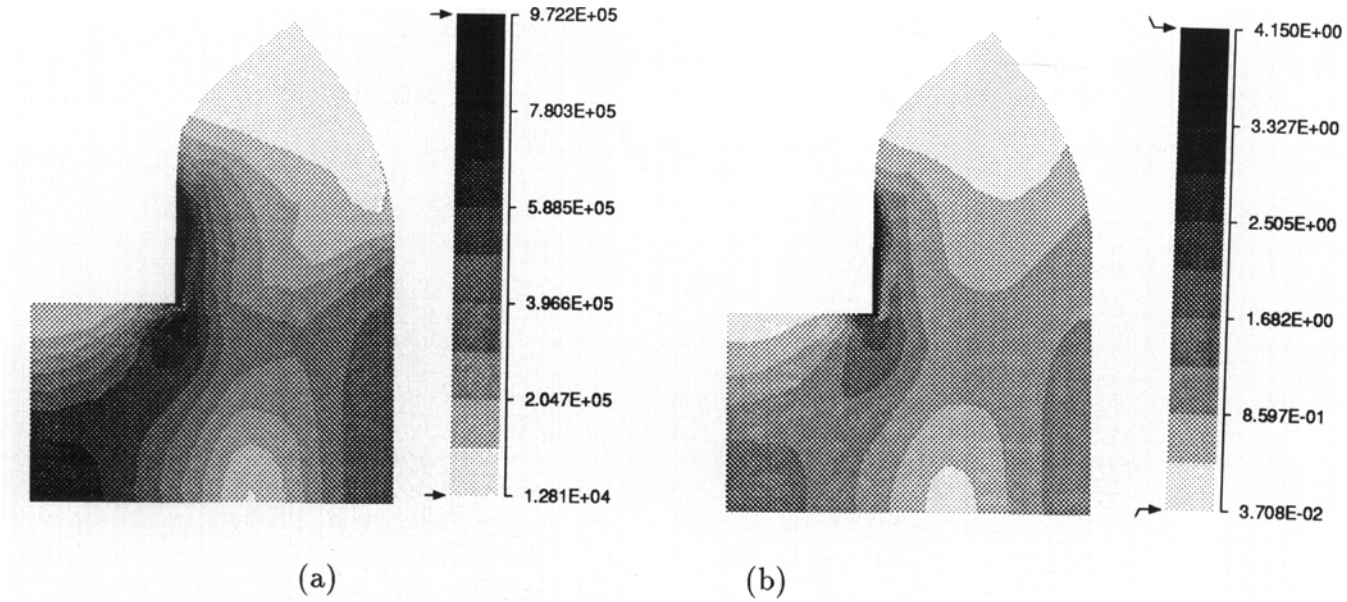

Fig. 9 (a) Equivalent stress. (b) Viscoplastic strain distribution in backward extrusion.

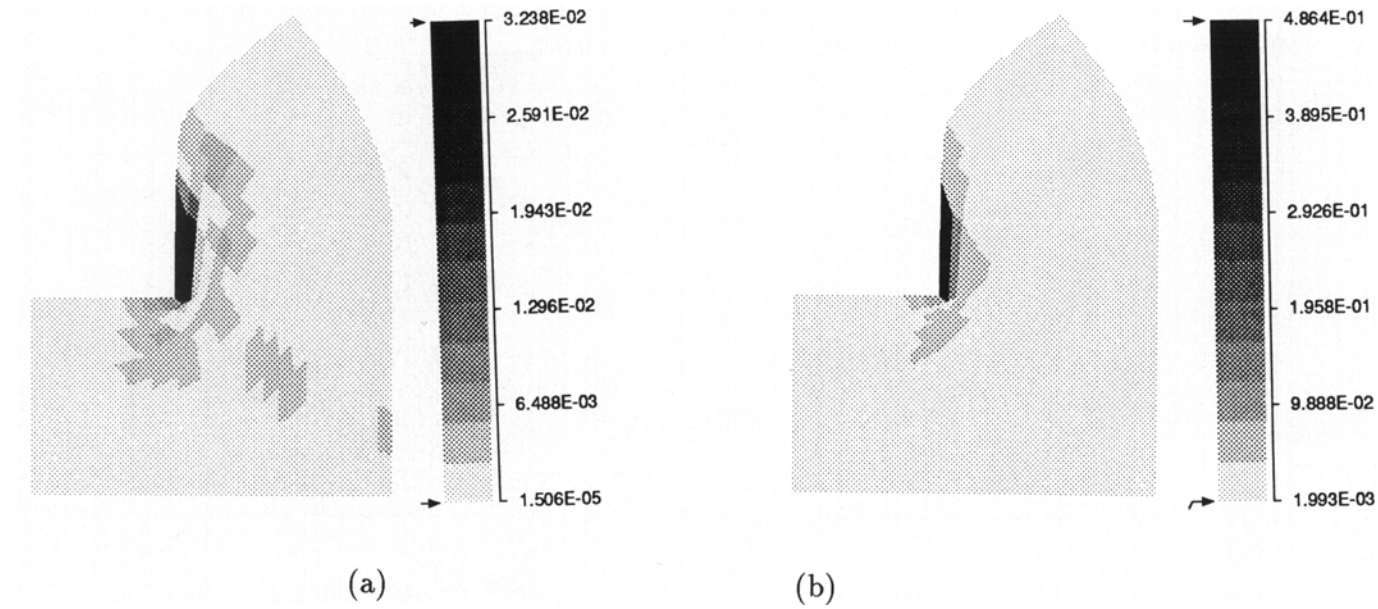

Fig. 10 Distribution of (a) incremental and (b) accumulated error.

4.2 *Forward Extrusion*

In this example, a wedge-shaped billet is forward extruded through an opening in a rigid die by a rigid punch, as shown in Fig. 12. Material properties are the same as in the previous example. The punch is assumed to move inward with a specified velocity of 1 in./s for a period of 0.5 s. To start, all of the nodes are maintained Lagrangian with the exception of the node that coincides with the die corner C. This node is initially assumed to be Eulerian and is glued to the corner of the die. During the deformation process, when an adjacent node B comes close to this Eulerian corner node C, B is made ALE. It is imparted a velocity such that it coincides with the corner node at the end of that time step, after which it becomes Eulerian and remains at the corner. After this step, node C is freed and becomes a Lagrangian node. Figures 13 and 14 show the comparison of maximum accumulated error for simulations with and without r-adaptation for $m = 1, n = 0$ and $m = 1, n = 1$, respectively. Adaptation starts at 5% punch stroke and is executed after every 2% stroke hence. The sudden rise in the error levels corresponds to a rise in the levels of plastic strain at the corner C. In spite of its failure at 7% stroke, in the example with $m = 1$ and $n = 1$, adaptation was successful in subsequently reducing the maximum error.

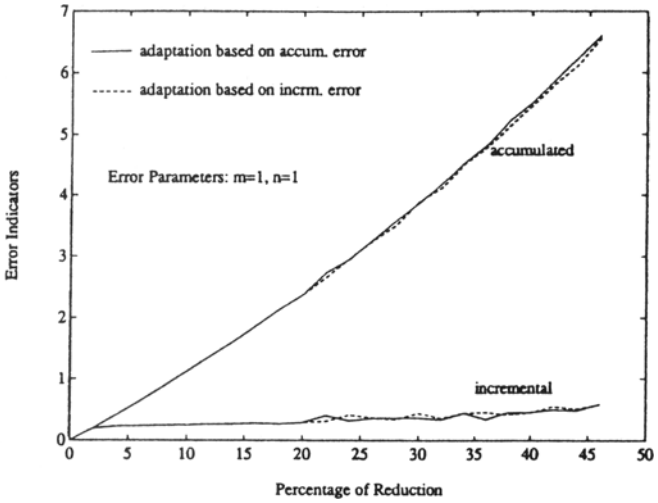

Fig. 11 Variation of error indicators with deformation.

The proximity of Eulerian and Lagrangian nodes at the die corner, at which the material undergoes a drastic change in flow direction, gives rise to nonconvex elements. As in the previous example, the combination of r-method and transfinite mapping with $m = 1$, $n = 1$ and adaptation based on accumulated error offered satisfactory simulation to a high degree of deformation. The value of the weight factor w has been varied from 0.3 near C through 0.95 away from the corner.

Figures 15 and 16 show the finite-element mesh and corresponding material configurations, respectively, at 30 and 50% punch stroke. Figure 17 depicts the equivalent stress and viscoplastic strain distribution in the material at 50% stroke, and Fig. 18 gives the corresponding distribution of incremental and accumulated errors. The incremental and accumulated errors of the total domain are plotted against percentage deformation in Fig. 19. In contrast with the backward extrusion example, the level of total accumulated error in the domain for adaptation based on incremental error was significantly lower than that with accumulated error.

5. Conclusion

In this study, an arbitrary Lagrangian-Eulerian finite-element model for large deformation analysis has been coupled with the capability of mesh adaptation based on equivalent vis-

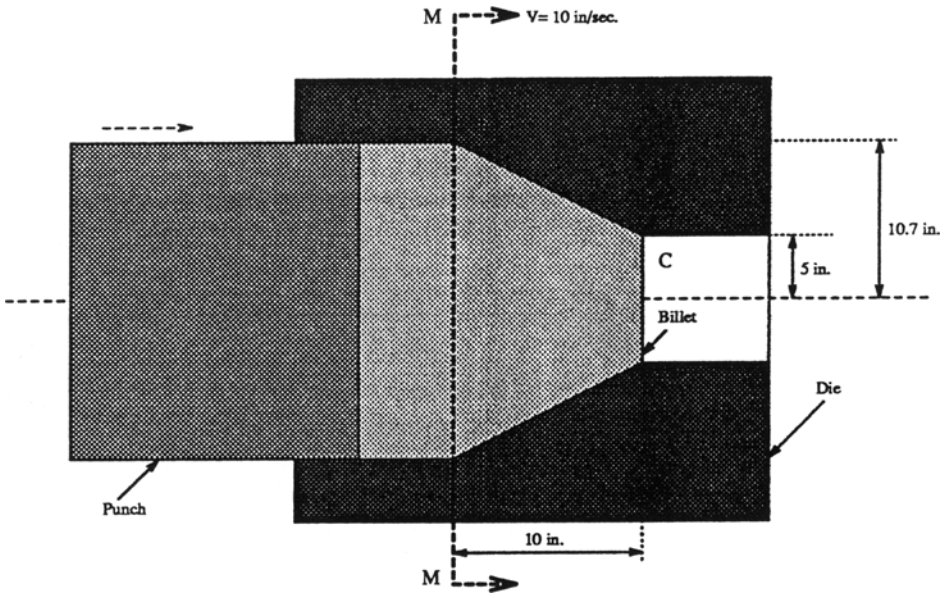

Fig. 12 Schematic of forward extrusion problem.

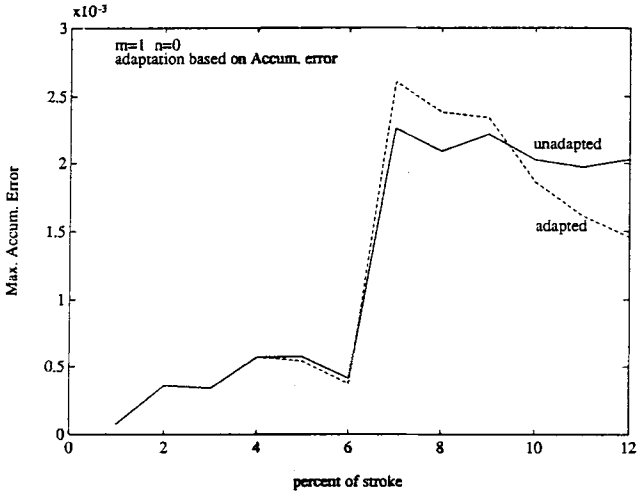

Fig. 13 Comparison of maximum accumulated error for adapted/unadapted forward extrusion ($m = 1, n = 0$).

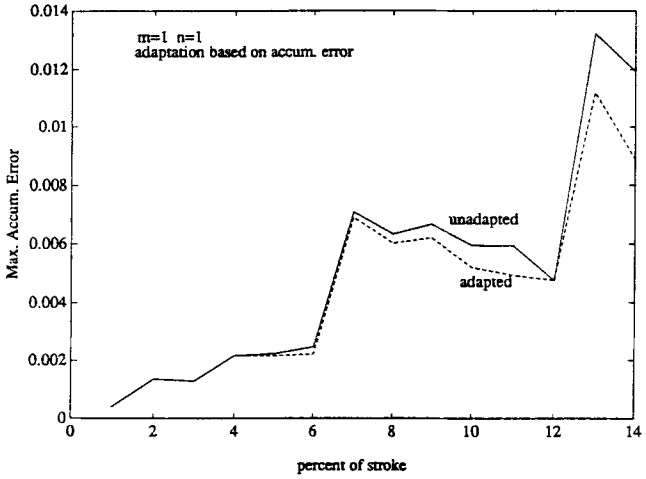

Fig. 14 Comparison of maximum accumulated error for adapted/unadapted forward extrusion ($m = 1, n = 1$).

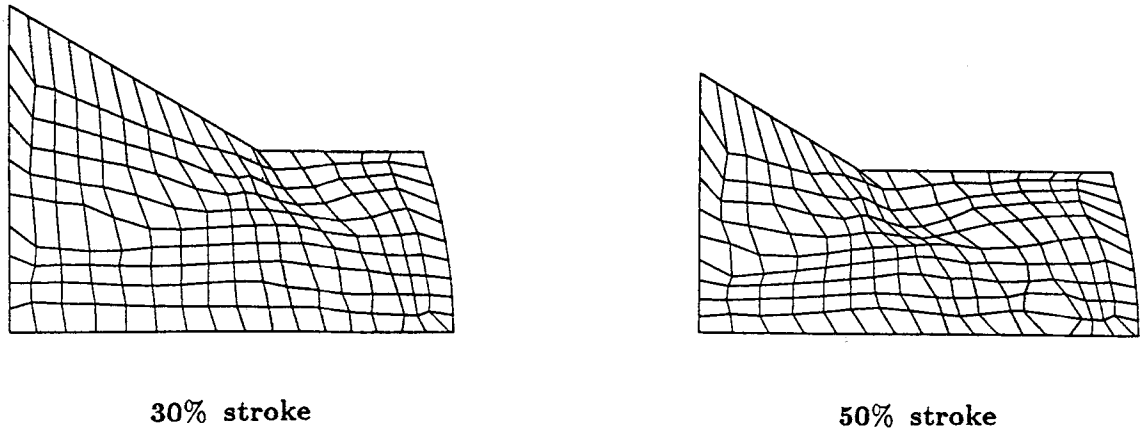

Fig. 15 Mesh movement in forward extrusion with *r*-adaptation and transfinite mapping.

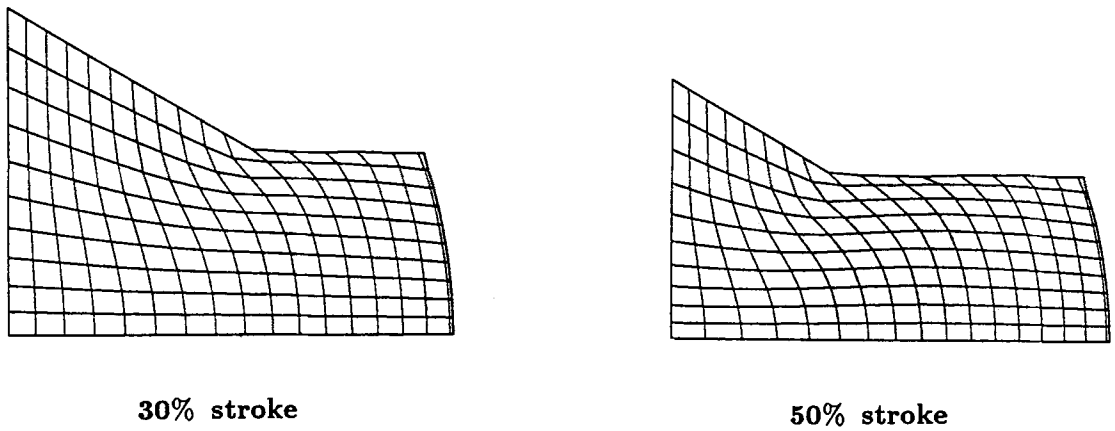

Fig. 16 Material motion in forward extrusion.

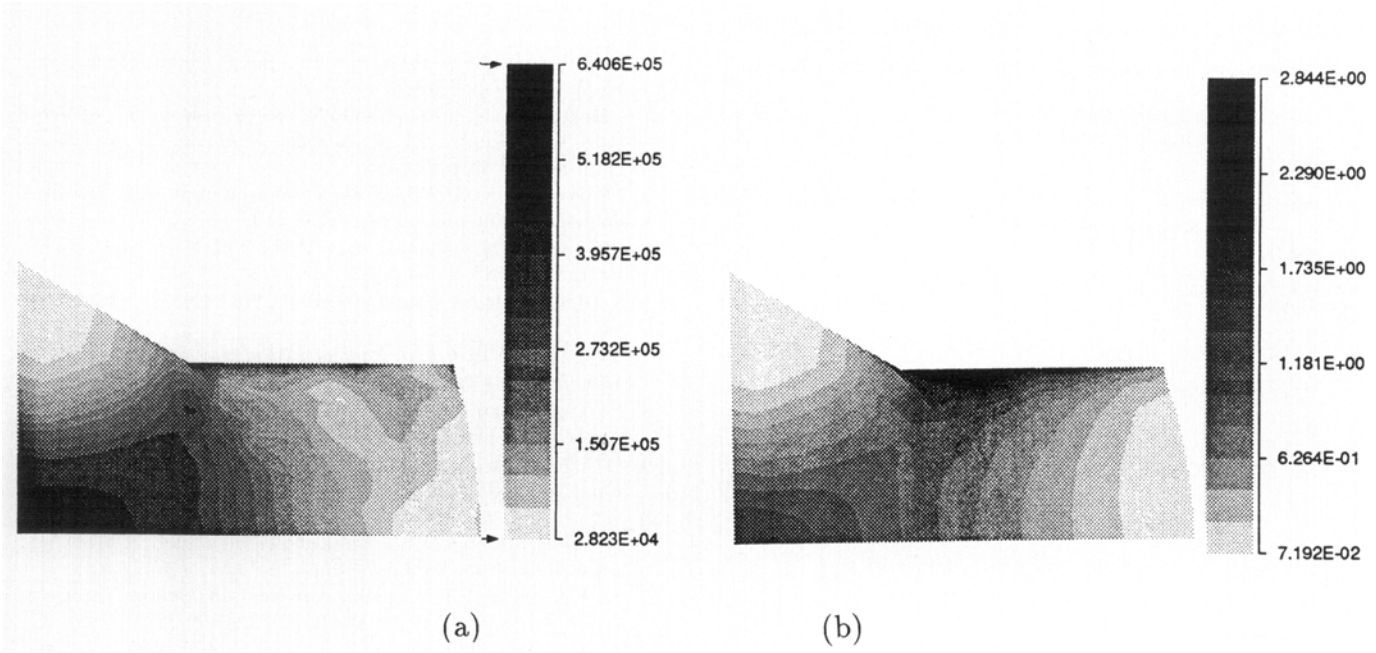

Fig. 17 Distribution of (a) equivalent stress and (b) equivalent plastic strain.

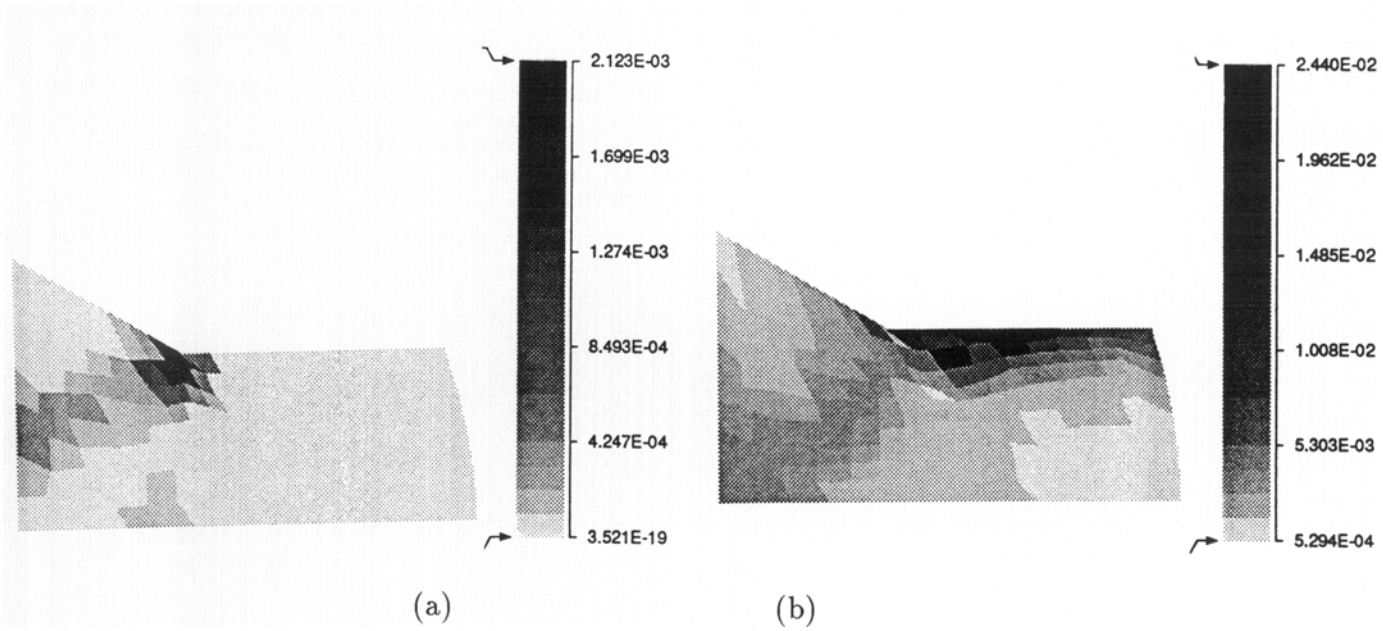

Fig. 18 Distribution of (a) incremental error and (b) accumulated error for $m = 1$, $n = 1$.

coplastic strain error estimators. The adaptive strategy uses the *r*-method of node relocation, which is best suited for the ALE model. Various choices of parameters m and n in the two error criteria (incremental and accumulated) resulted in different motions of the mesh. Comparison of results in the adapted case with those in the unadapted case exhibits a reduction in the maximum error in the domain. Severe element distortions near the punch edges, however, necessitated the coupling of *r*-methods with local automatic mesh generators. For this purpose, algebraic generators and transfinite mapping techniques were used. In the metal-forming simulations performed, the best results were obtained for a combination of parameters $m = 1$, $n = 1$ and adaptation based on the accumulated error together with transfinite mapping. Some instabilities in the mesh patterns were observed because of the local criterion for node relocation. A global optimization procedure may be effective in removal of these oscillations and is currently under investigation. Overall, it appears from this study, that a combination of the *r*-method with the ALE description has the potential for optimally maneuvering the finite-element grid during simulation.

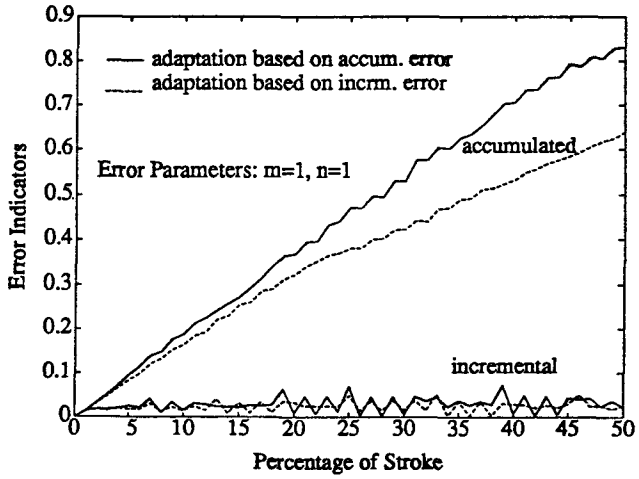

Fig. 19 Variation of error indicators with deformation.

Acknowledgments

Support of this work by the Army Research Office through Grant No. DAAL03-91-G-0168 and the National Science Foundation through NSF grant MSS-9009770 is gratefully acknowledged.

References

1. R.B. Haber, *Comp. Meth. Appl. Mech. Eng.*, Vol 43, 1984, p 277-292
2. W.K. Liu, T. Belytschko, and H. Chang, *Comp. Meth. Appl. Mech. Eng.*, Vol 58, 1986, p 227-246
3. J. Huetink, J. van der Lugt, and P.T. Vreede, in *Modelling of Metal Forming Processes*, J.L. Chenot and E. Onate, Ed., Academic Publishers, 1988, p 57-64
4. J.P. Ponthot, *NUMIFORM 89*, Thompson et al., Ed., Balkema Publishers, Rotterdam, 1989, p 203-210
5. S. Ghosh and N. Kikuchi, *Comp. Meth. Appl. Mech. Eng.*, Vol 86, 1991, p 127-188
6. S. Ghosh, *J. Mater. Shaping Technol.*, Vol 8 (No. 1), 1990, p 53-64
7. Y.-K. Hu and W.K. Liu, *Computer Modeling and Simulation of Manufacturing Processes*, MD-Vol 20, ASME, 1990, p 225-240
8. N. Kikuchi and J.H. Cheng, Rep. No. 87-14, Dept. Mech. Eng. Appl. Mech., University of Michigan, 1987
9. O.C. Zienkiewicz, Y.C. Liu, and G.C. Huang, *Int. J. Num. Meth. Eng.*, Vol 25, 1988, p 23-42
10. G.C. Huang, Y.C. Liu, and O.C. Zienkiewicz, *Modeling of Metal Forming Processes*, J.L. Chenot and E. Onate, Ed., Kluwer Academic Publishers, 1988, p 75-83
11. N. Kikuchi and T. Torigaki, *Advances in Inelastic Analysis*, AMD-Vol 88 PED-Vol 28, ASME, 1988, p 309-331
12. J.M. Bass and J.T. Oden, *Int. J. Eng. Sci.*, Vol 25, 1987, p 623-653
13. T. Torigaki, Ph.D. dissertation, The University of Michigan, 1989
14. N. Kikuchi, *Comp. Meth. Appl. Mech. Eng.*, Vol 55, 1986, p 129-160
15. A.R. Diaz, N. Kikuchi, and J.E. Taylor, *Sensitivity of Functionals with Application to Engineering Science*, V. Komkov, Ed., Springer-Verlag, Berlin, 1984
16. L. Demkowicz and J.T. Oden, *Int. J. Eng. Sci.*, Vol 24, 1986, p 55-68
17. S.K. Manna, M.S. thesis, The University of Alabama, 1991
18. J.H. Cheng and N. Kikuchi, *Int. J. Num. Meth. Eng.*, Vol 23, 1986, p 219-228